JOC The Journal of Organic Chemistry



Article

# Coordination Among Bond Formation/Cleavage in a Bifunctional-Catalyzed Fast Amide Hydrolysis: Evidence for an Optimized Intramolecular *N*-protonation Event

Leandro Scorsin, Ricardo Ferreira Affeldt, Bruno Surdi Oliveira, Eduardo Vieira Silveira, Matheus Santos Ferraz, Fábio Prá da Silva de Souza, Giovanni F. Caramori, Fredric M. Menger, Bruno S. Souza, and Faruk Nome

*J. Org. Chem.*, **Just Accepted Manuscript** • DOI: 10.1021/acs.joc.9b03383 • Publication Date (Web): 10 Mar 2020

# Coordination Among Bond Formation/Cleavage in a Bifunctional-Catalyzed Fast Amide Hydrolysis: Evidence for an Optimized Intramolecular *N*-protonation Event

Leandro Scorsin,[a] Ricardo F. Affeldt,[a] Bruno S. Oliveira,[a] Eduardo V. Silveira,[a] Matheus S. Ferraz,[a] Fábio P. S. de Souza,[a] Giovanni F. Caramori,[a] Fredric M. Menger,*[,b] Bruno S. Souza,*[,a] and Faruk Nome[a,†]

[a]Department of Chemistry, Federal University of Santa Catarina, Florianópolis, SC 88040-900, Brazil

[b]Department of Chemistry, Emory University, Atlanta, GA 30322, USA

[†]Deceased September 24, 2018.

## ABSTRACT

A density functional theory (DFT) computational analysis, using the ωB97X-D functional, of a rapid amide cleavage in 2-carboxyphthalanilic acid (2CPA), where the amide group is flanked by two catalytic carboxyls, reveals key mechanistic information: (a) General base catalysis by a carboxylate coupled to general acid catalysis by a carboxyl is not operative. (b) Nucleophilic attack by a carboxylate on the amide carbonyl coupled to general acid catalysis at the amide oxygen can also be ruled out. (c) A mechanistic pathway that remains viable involves general acid proton delivery to the amide nitrogen by a carboxyl while the other carboxylate engages in nucleophilic attack upon the amide carbonyl; a substantially unchanged amide carbonyl in the transition state; two concurrent bond-forming events; and a spatiotemporal-base rate acceleration. This mechanism is supported by molecular dynamic simulations which confirm a persistent key intramolecular hydrogen bonding. These theoretical conclusions, although not easily verified by experiment, are consistent with a bell-shaped pH/rate profile, but are at odds with hydrolysis mechanisms in the classic literature.

## INTRODUCTION

Isaac Newton recognized the presence of two types of variables: simple and composite. Simple variables (such as time, distance, and length) each consists of a single "pure" component. In contrast, composite variables are comprised of multiple contributors (called "elements") as occurs with entropy, resonance stabilization, ring-strain, and solvation.

The difference is easily appreciated when an attempt is made to compare, for example, distance and solvation. Distance is a straightforward parameter, whereas solvation is far more convoluted. It was for this reason that we have been interpreting organic and enzymatic reactivity in terms of two simple variables: distance and time ("spatiotemporal theory").[1] These two parameters seem preferable to "blends" of variables, especially when the goal is to understand complex chemical behavior.

We have previously supported experimentally the idea that rate accelerations of $>10^8$ occur when distances of <3 Å are imposed between two reactive atoms.[2] Stated in another way, proper orientation at short distances, less than the diameter of water, can lead to enzyme-like rates. An approximate relationship was derived (e.g. $E_a = cd^2$ where $E_a$ is the activation energy, c the speed of light, and d the interatomic distance)[3] that additionally affirms the remarkable sensitivity of rate to distance. One of our published experimental examples, shown in Figure 1, serves to illustrate the concept.[4] This amide hydrolyzes so rapidly that, owing to its contact distances <3 Å from two carboxyls, the amide cannot be isolated intact at 35°C and pH 4. Compare this reactivity with that of an "ordinary" amide, such as benzamide, having a half-life of 3 hours at 85°C in 5.9% $H_2SO_4$.[5]

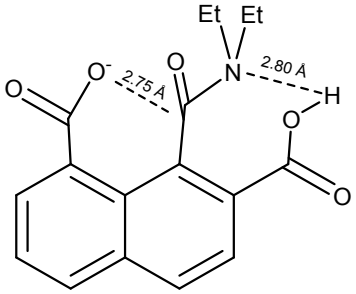


**Figure 1**. 2-carboxy-*N,N*-diethylnaphthalamic acid, an amide which decomposes with a half-life of 20 seconds at pH 4, 35°C. The interatomic distances were determined by DFT calculations. See reference 4 for details.

Spatiotemporal notions extend to the enzymes themselves. For example, citrate synthase holds the enolizable methyl group of acetyl-CoA a distance of ca. 2.9 Å from the carbonyl group that the methyl carbon is destined to attack. Aspartic proteases, such as HIV-1 protease, are enzymatic systems that operate via two spatially directed carboxyl groups; a $10^{10}$-fold acceleration ensues.[6,7] A favored mechanism has an aspartate anion removing a proton from a nucleophilic water molecule as the water adds to the amide carbonyl group. Simultaneously, the second aspartate, in its conjugate acid form, donates a proton to the amide's carbonyl group. The resulting tetrahedral intermediate, with a *gem*-diol functionality, then collapses to the cleaved amide. Huge rates associated with this mechanism can be

ascribed to nearly ideal contact geometries. Both experimental and computational observations bear this out.[8] Among the many X-ray pictures of complexes between an enzyme and its substrate-analog, one generalization stands out (except in cases where the substrate analog distorts the active site): Short distances are usually imposed upon the active conformations.[9]

Carboxyl groups, the key functionalities of the discussion herein, are well known to accelerate amide hydrolysis in intramolecular systems. For example, at pH 3 the hydrolysis of phthalamic acid is about $10^5$ faster than the hydrolysis of benzamide.[10] *N*-methylmaleamic acid has a half-life of 3 h at 39°C below pH 2 where the carboxyl group is fully protonated (the carboxylate substituent is noncatalytic).[11] A Kemp's triacid derivative, which has an enzyme-like half-life of only 8 min. at pD 7.02 and 21.5°C, shows that a protease could in principle achieve full catalytic power by having only two properly positioned carboxyl groups.[12]

We discuss herein 2-carboxyphthanilic acid (2CPA, 1 in Scheme 1) from a spatiotemporal perspective. Decades ago Morawetz, in their classic paper, demonstrated an intramolecular bifunctional-catalyzed amide hydrolysis, with 2CPA existing in three protopic states (1, 1a, and 1b).[13] By comparison, phthalanilic acid (2), 2-(benzamide)benzoic acid (3) and 4-carboxyphthalanilic acid (4) all react slowly, verifying the bifunctional nature of the 2CPA reaction.

**Scheme 1**. Protonic states of carboxyphthalanilic acid (2CPA), 1, 1a and 1b.[12] Also shown are the structures of much more stable related compounds.

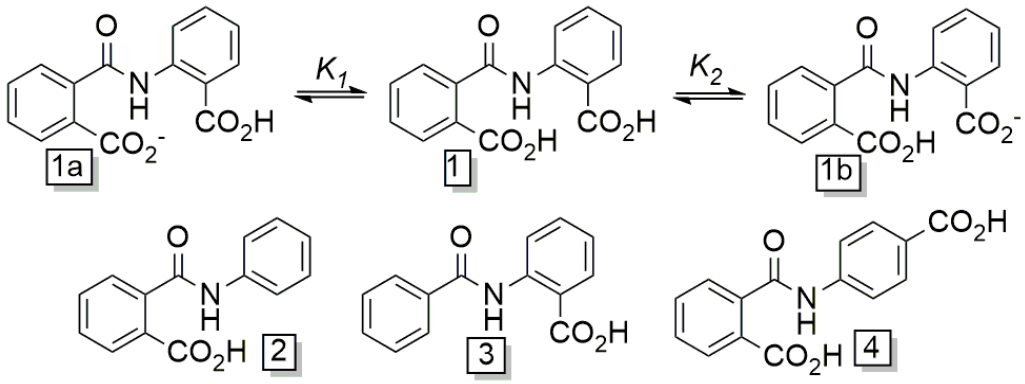

## RESULTS AND DISCUSSION

We now report a mechanistic study on the 2-carboxyphthalanilic acid (2CPA) hydrolysis reaction. Both proton transfer and nucleophilic attack occur in the cleavage. Coordination and timing between the two reaction modes, the subject of prime interest, was investigated computationally. As will be seen, in a sharp disagreement with the conclusions of Morawetz, protonation at the N atom, but not the O of the carbonyl group, is revealed to play a role in the amide cleavage.[13]

2CPA hydrolysis initially produces phthalic anhydride (PAn) and anthranilic acid (AA) shown in Scheme 2. Under acidic conditions, the initially formed anhydride rapidly hydrolyzes to phthalic acid (PAc).[14,15] Figure 2 shows successive UV-Vis absorption spectra at pH 3.5 for 2CPA decomposition. As can be seen, the UV-Vis spectral differences allow the easy monitoring of the reaction progress and determination of first-order rate constants. The sharp isosbestic point testifies to a simple reaction mechanism and purity of the reactants.

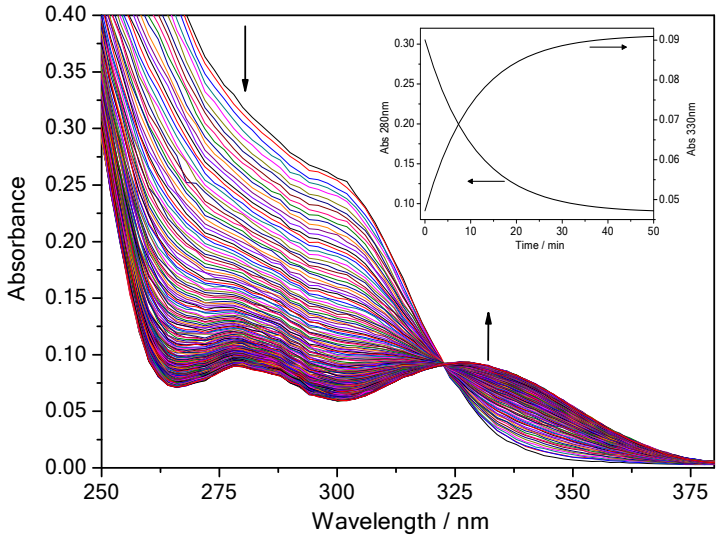


**Figure 2**. Successive UV-Vis absorption spectra for decomposition of 2CPA at 25°C, pH 3.5. The inset shows the absorbance variation at 280 nm (left) and 330 nm (right) which are due phthalate ($PAc^-$) and anthranilate ($AA^-$), respectively.

Observed rate constants $k_{obs}$ in $s^{-1}$ for the cleavage of 2CPA at 25.0°C as a function of pH and pD are given in Figure 3. The bell-shaped plot supports and confirms the work of Morawetz over fifty years ago. At pH 5 the half-life is about 100 min. For comparison, hydrolysis of a simple amide such as benzamide is not observable at pH 5. As the pH is

lowered below pH 5, the rate rises uniformly until its maximum is reached near pH 3.5. Further pH reduction decreases the rate to give the left side of the bell-shaped pH/rate profile. Full spectral data are given in the Supporting Information (SI).

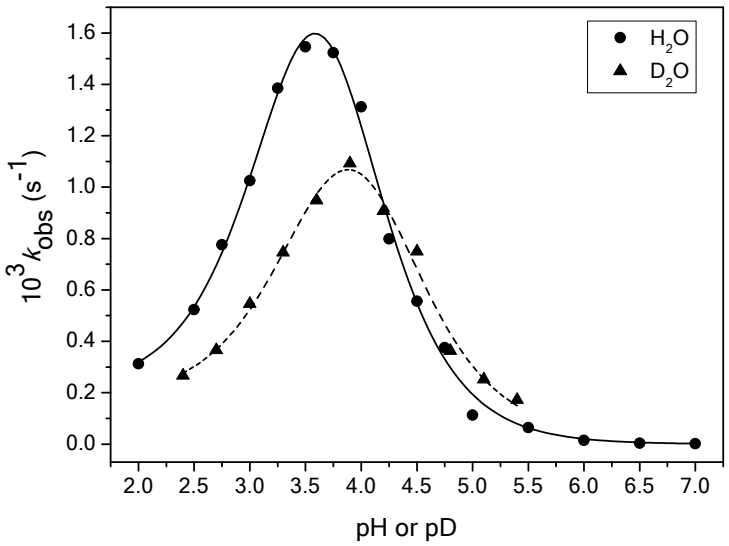


**Figure 3**. First-order rate constants $k_{obs}$ vs. pH or pD for the decomposition of 2CPA at 25°C. Curves are nonlinear fittings using the equation given in the SI.

Nonlinear fitting of the pH/rate profile plot in Figure 3 according to Scheme 2 provides p$K_{a1}$=3.3; p$K_{a2}$=3.7; $k_1$=2.1x10$^{-4}$ s$^{-1}$; $k_2$=4.0x10$^{-3}$ s$^{-1}$; and $k_3$=1.4x10$^{-5}$ s$^{-1}$. The bell-shaped curve can be understood by starting at pH 5, where 1c predominates, and moving to the left. Lacking the possibility of intramolecular acid catalysis, the rate at pH 5 corresponds to a slow $k_3$. As the pH is lowered, 1a, possessing both a carboxyl and a carboxylate, makes its presence known kinetically. The associated rate constant, $k_2$, is fast and consistent with a bifunctional catalysis where the carboxylate functions as a nucleophile and the carboxyl as a general acid. A further pH drop (3.5 to 2.0) creates the non-ionic diacid species, 1, that is associated with a slow $k_1$ owing to the lack of a good anionic nucleophile to attack the amide carbonyl. In summary, the impressive catalytic effect (i.e. an amide that cleaves with a 7 minute half-life) arises from a bifunctional catalysis contributed by the two carboxyl entities.

**Scheme 2.** Species involved in the hydrolysis of 2-carboxyphthalanilic acid (2CPA).

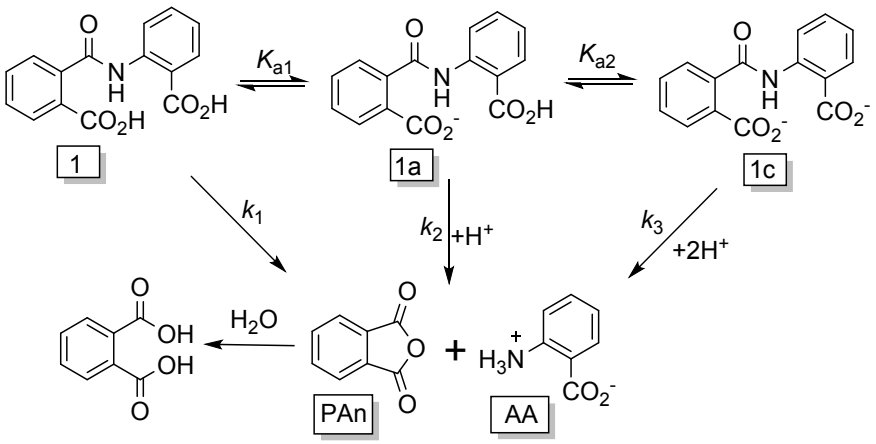


Mechanistic mysteries persist. Does the nucleophilic carboxylate directly attack the amide carbonyl, or is a carboxylate a general base that removes a proton from a water molecule that in turn serves as the nucleophile? And do proton transfers, which are obviously involved in the course of the mechanism, occur simultaneously with such an attack on the amide carbonyl, or are these separate steps? To what amide atom, nitrogen or oxygen, is the carboxyl proton delivered? Is there an intermediate, such as a tetrahedral intermediate, involved in the reaction? What distances are involved in the transition state (or transition states)? Such questions are addressed below with the aid of DFT calculations (see computational details in the experimental section). Four mechanistic schemes are considered and compared.

Direct attack by a water molecule with intramolecular catalysis was considered first as similar reactions were reported for ester hydrolysis in related systems. [16–18]. The attack is general-base catalyzed by a well positioned carboxylate group in a transition state with a 7-membered ring. This is accompanied by proton delivery from the general acid carboxyl group to either (*i*) the carbonyl oxygen (TSw-1) or (*ii*) nitrogen atom (TSw-2) (Scheme 3). In both cases, the final products are PAc and $AA^-$. Activation free energies, calculated by taking the difference of the Gibbs free energy of the transition states and the reactant 1a coordinated to a water molecule (see structure 1a.$H_2O$ in the SI), are 29.9 kcal $mol^{-1}$ and 32.6 kcal $mol^{-1}$, respectively, more than 10 kcal $mol^{-1}$ higher than the experimental free activation energy of 20.6 ± 2.1 kcal $mol^{-1}$ at 25 °C (see the Eyring plot in the SI). It should be noted that these computational energies are underestimated as pointed out elsewhere.[19] Therefore, participation of a nucleophilic water can be ruled out.

**Scheme 3.** Decomposition of 1a involving a nucleophilic water molecule with simultaneous general base and general acid assistance to the oxygen (TSw-1) or nitrogen (TSw-2) atoms, respectively. Ball-and-stick representations of transition states and respective IRC plots are given in the SI (see Figures S1 and S2). Cartesian coordinates are given in the SI.

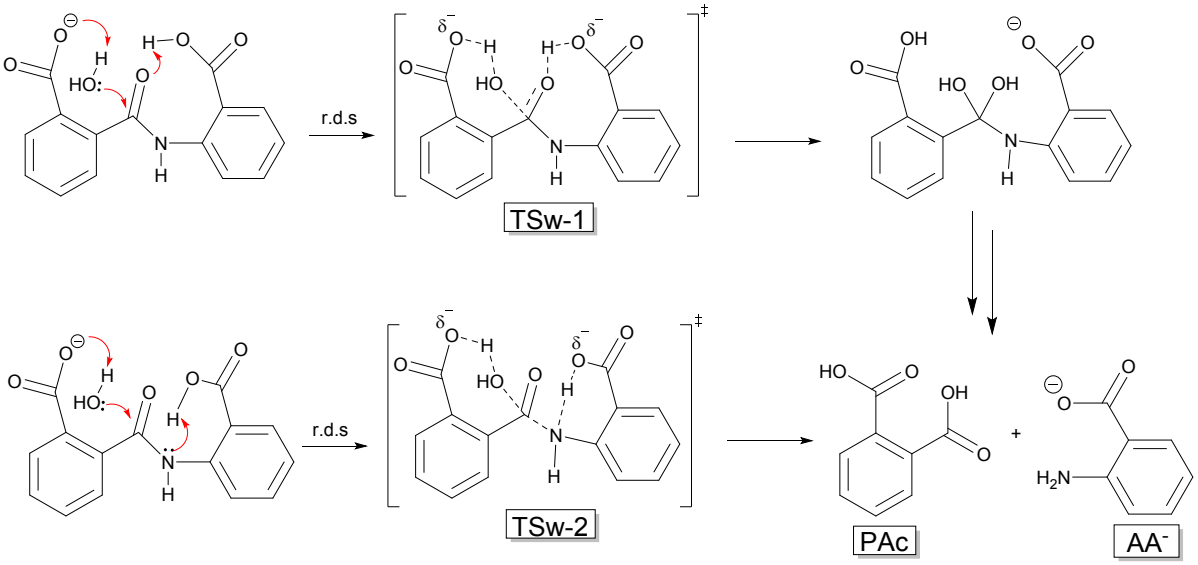


We then analyzed the carboxylate attack on the amide carbonyl. This attack is accompanied by protonation of the negative charge developed on the amide oxygen by the neighboring carboxyl group (Scheme 4). The activation free energy for TS-1, only 13.8 kcal $mol^{-1}$ relative to 1a, leads to a 5-membered lactone-type structure I-1, itself 12.9 kcal $mol^{-1}$ above reactant 1a. The 5-membered ring incorporates the classic "tetrahedral intermediate" configuration commonly postulated on reactions of carboxylic acid derivatives. The question now resides on decomposition of I-1 which certainly must involve activation of the leaving group by protonation. This can occur by (*i*) a four membered transition state with a proton coming from the neighboring –OH group (*path a*, TS-2) or (*ii*) through participation of a water molecule which delivers a proton, via a six membered transition state, to the N atom while removing a proton to restore the carbonyl group (*path b*, TS-3). Both transition states lead to PAn+$AA^-$ and the $\Delta G^{\ddagger}$'s are 46.9 kcal $mol^{-1}$ and 34.4 kcal $mol^{-1}$ for TS-2 and TS-3, respectively, much too high to render *path a* and *path b* as likely mechanisms.

**Scheme 4.** Decomposition of 1a involving intramolecular proton transfer to carbonyl oxygen. For TS-1, I-1, TS-2 and PAn+$AA^-$ the reference is 1a while for TS-3 the reference is 1a.$H_2O$. For species involved in *path c* the reference is I-2. The values given are DFT activation free energies in kcal $mol^{-1}$. The ball-and-stick models of all species are given in the SI.

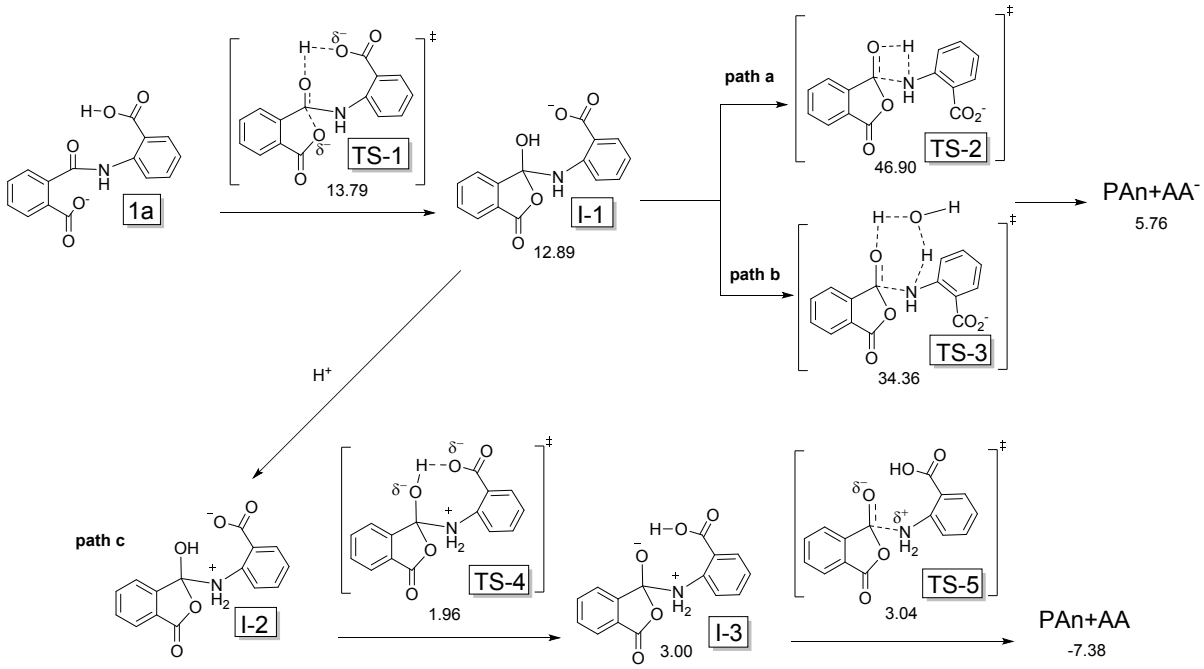


In seeking a plausible path for the collapse of I-1, we hypothesized that this species can readily protonate via hydronium ions in solution, thereby entering *path c* in Scheme 4. Nitrogen protonation of I-1 led to the tetrahedral intermediate I-2 which is then converted to products PAn+AA through TS-4, I-3 and TS-5. The intrinsic reaction coordinate (IRC) curves for these steps are given in Figure S3 and confirm that all species are connected. The computed activation free energy for the highest barrier (TS-5) is only 3.04 kcal $mol^{-1}$, indicating that I-2 is quickly converted to products in an irreversible, barrier-less reaction.

The intermediate I-1 can be converted back to 1a or be protonated by hydronium ions in a thermodynamically favorable diffusion controlled reaction and, therefore, does not accumulate. Hence it is possible to apply the steady state approximation to I-1. It follows that the apparent rate constant for conversion of 1a into PAn+AA via *path c* is given by Eq. 1, where $k_4$ and $k_{-4}$ are first-order rate constants for the forward and reverse reaction involving 1a and I-1, respectively, while $k_p$ is the second order rate constant for the diffusion controlled protonation of I-1 (approximately $10^{10}$ $M^{-1}s^{-1}$). Using the Eyring equation one can calculate $k_4$ and $k_{-4}$ from the DFT activation energies. Since the observed rate constant $k^{O}_{obs}$ is the product of $k^{O}_{app}$ and the molar fraction of 1a (Eq. 2), it is possible to simulate the pH rate profile for the mechanism involving I-1 and I-2. As can be seen in Figure 4, the simulated pH rate profile is sigmoidal as opposed to the bell-shaped plot obtained experimentally. It is therefore concluded that the mechanisms in Figure 4 are unlikely.

$$k_{app}^{O} = \frac{k_4 k_p [H_3O^+]}{k_{-4} + k_p [H_3O^+]} \qquad \text{Eq. 1}$$

$$k_{obs}^{O} = k_{app}^{O} \frac{1}{1 + \frac{[H_3O^+]}{K_{a1}} + \frac{K_{a2}}{[H_3O^+]}} \qquad \text{Eq. 2}$$

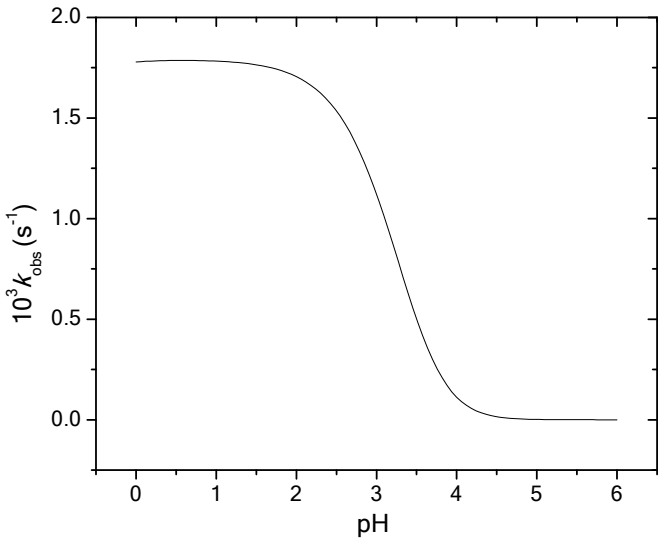


**Figure 4.** Simulated pH rate profile for the stepwise decomposition of 1a involving *path c* in Scheme 4. The curve was simulated using Eq. 2 with $K_{a1}$=5x10$^{-4}$, $K_{a2}$=2x10$^{-4}$, $k_4 = 477 s^{-1}$, $k_{-4} = 133x10^{10}$ $s^{-1}$, $k_p$=1x10$^{10}$ M$^{-1}$s$^{-1}$ at 298 K.

As initial amide carbonyl protonation in Scheme 4 was not viable, we searched for 1a decomposition mechanism involving nitrogen protonation as previously demonstrated to occur with 2-carboxyl-*N,N*-diethylnaphthalamic (see Figure 1).[4] Figure 5 shows the ball-and-stick models of the calculated species found in this reaction path. In order to better visualize the bond-forming and bond-breaking processes, the IRC plot for conversion of 1a into PAn+AA$^-$ is given in Figure 6.

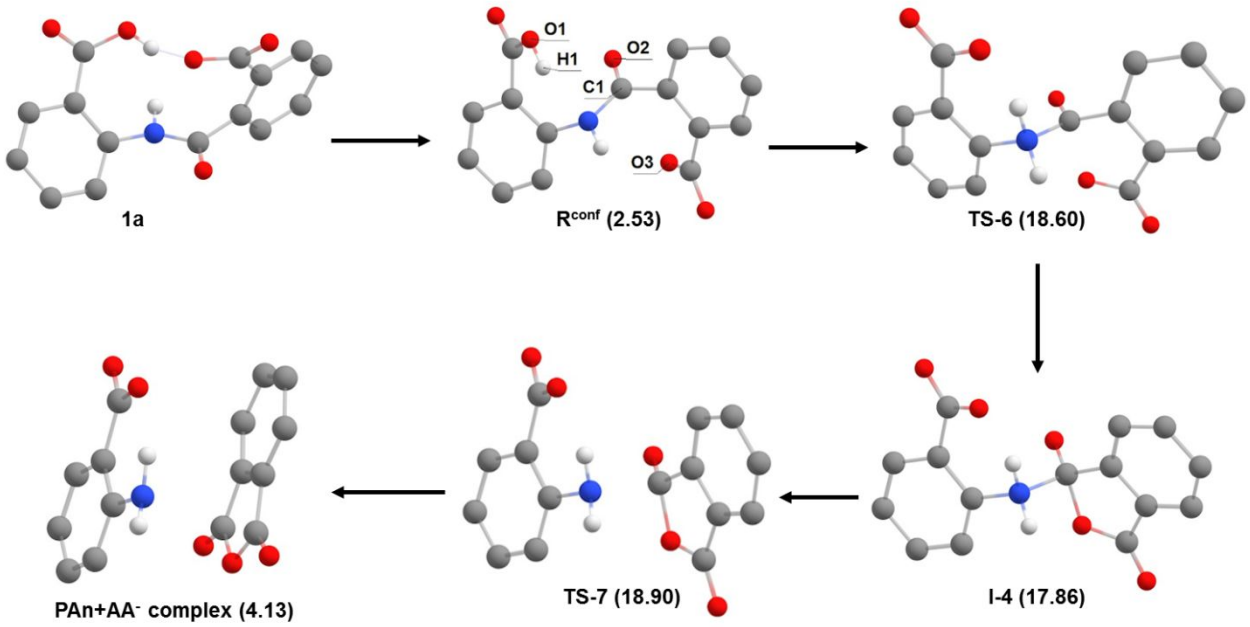


**Figure 5.** Ball-and-stick models of the stationary points found for the decomposition of 2CPA involving intramolecular proton transfer to nitrogen. Values in parenthesis are the computed free energies (kcal $mol^{-1}$) relative to 1a. Hydrogens bound to carbon atoms were omitted for clarity purposes. See the IRC curve of Figure 6 for a detailed description of the variation of bond lengths along this reaction path.

The pathway for 1a decomposition shown in Figure 5 involves the stepwise C1-O3 bond formation and C1-N cleavage. The reaction starts with the reactive conformer $R^{conf}$, which is converted to I-3 thought transition state TS-5. As can be seen in the IRC analysis, in TS-5 protonation of the amide nitrogen from the neighboring -$CO_2H$ group is well advanced (N-H1 and O1-H1 interatomic distances are 1.08 Å and 1.54 Å, respectively), the C1-N double bond character has been considerably diminished (C1-N interatomic distances is 1.53 Å versus 1.36 Å in 1a), and an incipient bonding between the carboxylate and the amide carbonyl carbon is observed (C1-O3 = 1.91 Å). In the high energy intermediate I-3 the C1-O3 and C1-N bonds are almost equidistant (1.55 Å and 1.60 Å, respectively). The intermediate is decomposed through TS-6 with the main geometrical changes are the increase in the C1-N distance and decrease in the C-O3 bond-length. The whole process occurs with a surprisingly static amide carbonyl (C1-O1 is 1.26 Å in I-3 versus 1.22 Å in 1a).

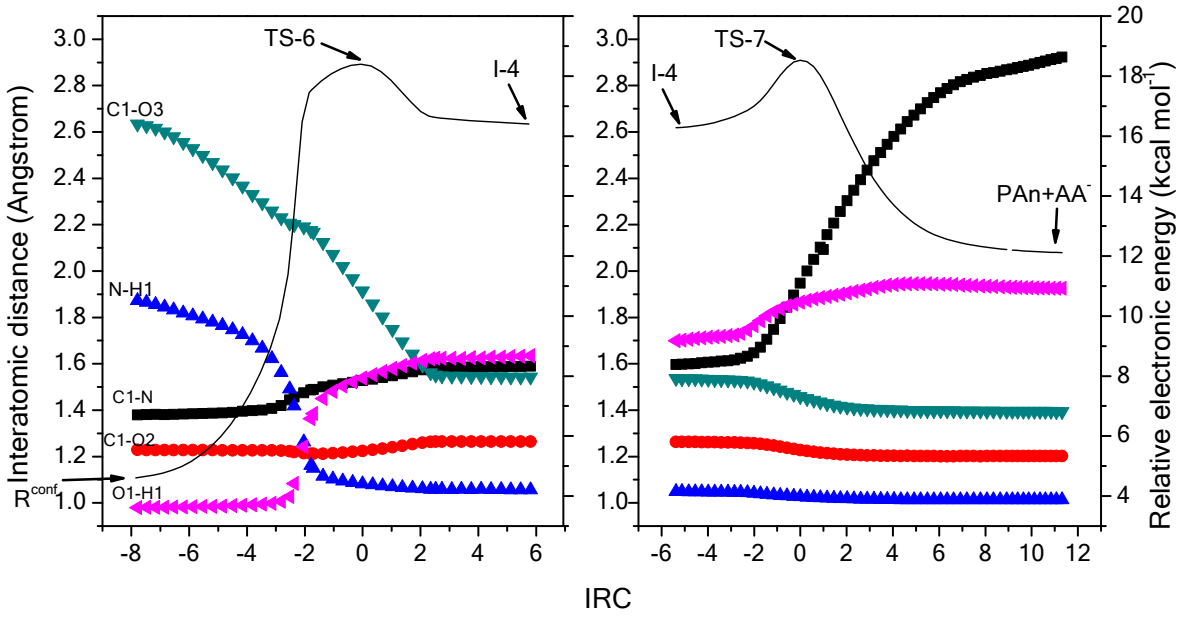


**Figure 6.** Variation of bond lengths (dotted lines) and electronic energies (solid lines) along the IRC for the decomposition of 1a via intramolecular *N*-protonation. The panels on the left and on the right correspond to conversion of $R^{conf}$ →I-4 and I-4 → PAn+$AA^-$, respectively. The arrows indicate the position of transition states, located at 0 bohr, $R^{conf}$ and I-4. The electronic energy was computed taking 1a as reference. Atom numbering according to Figure 5.

Proton transfer in the mechanism involving intramolecular *N*-protonation is consistent with the solvent isotope effect of 1.90 observed in Figure 3. An attainable energy of 18.6 kcal $mol^{-1}$ is involved in the first step (TS-6), while the subsequent decomposition of I-4 occurs thorough TS-7, which lies 18.9 kcal $mol^{-1}$ up in energy from 1a. This value is in good agreement with the experimental one, the small differences in which are attributable to explicit solvent effects which were not included in our calculations. The intermediate lies only 0.6 and 1.0 kcal $mol^{-1}$ below TS-6 and TS-7, respectively. Therefore it is of fleeting existence. It is either converted back to 1a or processed further into products.

The computed product in Figure 5 is an interacting complex formed by PAn+$AA^-$. The Gibbs free energy of this complex is 4.13 kcal $mol^{-1}$ above that of 1a. At first glance this indicates that the equilibrium is shifted towards the reactant. However, one should bear in mind that in solution PAn is quickly converted to phthalic acid[14,15] consequently shifting the equilibrium towards 1a decomposition.

Experimentally, the two competing paths for 1a hydrolysis, namely *N*- and *O*-protonation, are difficult to delineate. However, a kinetic analysis using the activation energies from the DFT results helps elucidate the question. Applying the steady state approximation to I-3 it follows that the apparent rate constant for conversion of 1a into

PAn+AA$^-$ *via* I-3 is given by Eq. 3, where $k_5$ and $k_{-5}$ are first-order rate constants for the forward and reverse reactions involving 1a and I-4, respectively, and $k_6$ is the first order rate constant for conversion of I-4 to products passing through TS-7. The simulated pH rate profile of Figure 7 clearly resembles the bell-shaped experimental curve shown in Figure 3. Moreover, at pH 3.5 the reaction involving *N*-protonation is approximately 50-fold faster than *O*-protonation via reaction *path c* in Scheme 4. Thus, contrary to many speculations in the classical literature, *N*-protonation in amide hydrolysis prevails.

$$k_{app}^{N} = \frac{k_5 k_6}{k_{-5} + k_6} \qquad \text{Eq. 3}$$

$$k_{obs}^{N} = k_{app}^{N} \frac{1}{1 + \frac{[H_3O^+]}{K_{a1}} + \frac{K_{a2}}{[H_3O^+]}} \qquad \text{Eq. 4}$$

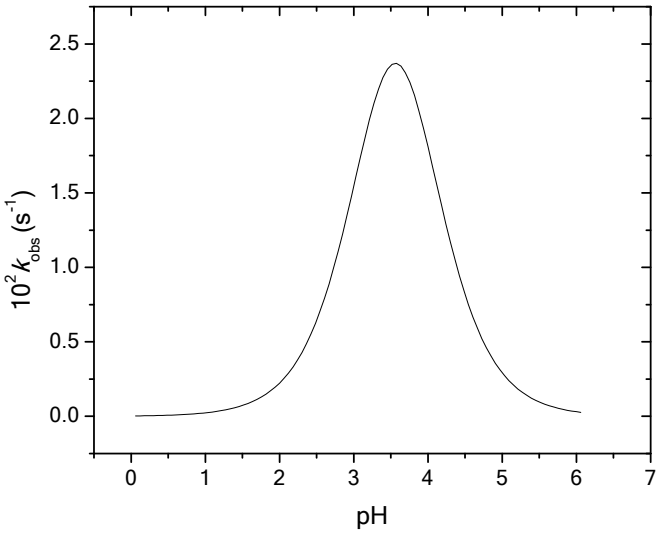


**Figure 7.** Simulated pH rate profile for the decomposition of 2CPA involving *N*-protonation according to Figure 5. The curve was simulated using Eq. 4 with $K_{a1}$=5x10$^{-4}$, $K_{a2}$=2x10$^{-4}$, $k_5 = 0.144\ s^{-1}$, $k_{-5} = 181x10^{10} s^{-1}$, $k_6 = 108x10^{10} s^{-1}$ at 298 K.

The question remains as to the exact source of the observed rate acceleration. Since the unsubstituted amide is inert to acetate, even at high concentrations, it is obvious that intramolecularity is crucial. But this is a low-information statement, and one would prefer a deeper understanding. In line with spatiotemporal considerations, mentioned in the beginning of this paper, we believe that truly fast rates in solution, e.g. those associated with enzyme catalysis (>10$^8$), arise from imposed separations among reacting atoms that approach van der

Waals distances. We have published elsewhere numerous examples of spatiotemporal effects where contact distances lead to enzyme-like accelerations.[1,2] It was thus incumbent on us to examine the geometric properties of the reactive conformer $R^{conf}$ shown in Figure 8. This structure was uncovered was found by following the IRC in the reverse direction from TS-5 (see Figure 6) followed by full optimization.

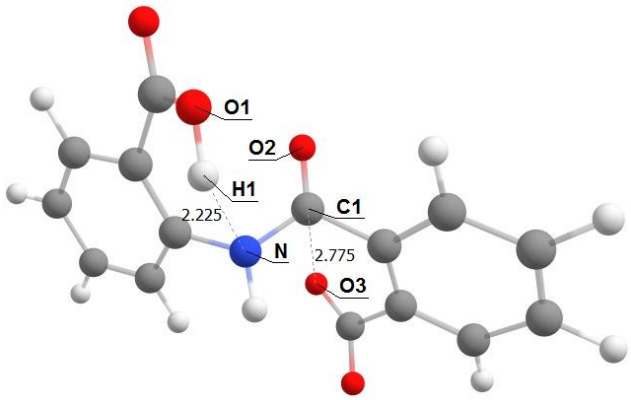


**Figure 8.** Structure of the reactive conformer $R^{conf}$ involved in decomposition of 1a via intramolecular *N*-protonation. Values are interatomic distances in Angstroms.

The conformer $R^{conf}$ is a local minimum only 2.52 kcal $mol^{-1}$ above the 1a global minimum. The interatomic distance between the hydrogen atom of the carboxyl group and the amide nitrogen is 2.23 Å. More importantly, the nucleophilic carboxylate oxygen O3 is separated from the amide carbonyl carbon electrophile by only 2.78 Å, close to the diameter of water. In addition, the nucleophilic O3 is directly above the plane of the amide, leading to a very significant orbital overlap (∠O3···C1=O2 is 106.45 °). Besides, the C1-N bond length of 1.37 Å is slightly longer than the typical length observed in amides. The spatial conditions for a fast reaction according to spatiotemporal theory are clearly in place.

In order to access the life-time of reactive 2CPA conformers, we performed molecular dynamics simulations on 200 ns time scales of $R^{conf}$ with explicit solvation using the TIP3P water model. In total, 400,000 frames were obtained. A hydrogen bond analysis revealed that the N-H1 interatomic distance is equal or less than 3.0 Å in 14.21 % of the frames, and the average distance is 2.69 Å. A similar analysis for O2-H1 revealed that this intramolecular hydrogen bonding is much less frequent, being observed in only 0.41 % of the frames (the average distance is 2.77 Å). These results indicate that 2CPA is very prone to the *N*-protonation reaction path. In addition, analogously to the near attack conformer concept introduced by Bruice several years ago,[20] we analyzed the probability of finding reactive states that simultaneously meet the following criteria: N-H1 and C1-O3 interatomic distances

smaller than 3.0 Å and a ∠O3···C1=O2 angle within 107.0 ± 5.0º. These criteria are simultaneously observed in 1.61 % of the frames, whereas the average lifetime for these states is 1.2 ps. Hence, the temporal component of a spatiotemporal effect is not ideal. Since reactive sites are of fleeting existence among other conformations, a proper contact distance was present but not permanently enforced. If the rotations about the single bonds had been restricted, as they are at active sites of enzymes, true enzyme-like accelerations would, we feel certain, have been achieved.

## EXPERIMENTAL SECTION

**Materials.** All reagents were analytical grade. Deionized water was used in all measurements. The following buffering systems were used in the kinetic studies: chloroacetic acid (pH 2.00-3.75), acetic acid (pH 4.00-5.50) and Bis-Tris (pH 6.00-7.00). All buffered solutions had concentrations of 0.01 mol.L$^{-1}$ and the pH and pD values were adjusted with NaOH/HCl aqueous solutions or NaOD/DCl in $D_2O$, respectively.

**Methods.** UV-Vis spectra were taken in a Cary 50 spectrophotometer coupled to a Varian PCB 1500 thermostatic bath with Peltier water system. Kinetic runs for hydrolysis of 2-carboxyphthalanilic acid (2CPA) were carried out under first-order conditions. The reactions were started by adding 10 µl of a 0.01 M stock solution of 2CPA in acetonitrile to 3 ml of the aqueous buffered solutions in a quartz stoppered cuvette (10 mm path length). The appearance of anthranilic acid from 2CPA was followed by the increase in absorbance at 330 nm. All reactions gave strict first-order kinetics over more than five half-lives. Unless otherwise specified, reactions were carried out at 25ºC. Activation parameters were determined from 25°C to 55ºC using the Eyring equation with $k_2$ values.

**Computational.** DFT calculations were performed using the ωB97X-D functional[21,22] with the 6-311++G(d,p)[23–27] basis set using GAUSSIAN 09 A.02 package[28] implemented in Linux operating systems. The default parameters for convergence, were used; convergence on the density matrix was 10$^{-9}$ atomic units, the threshold value for maximum displacement was 0.0018 Å, and the maximum force 0.00045 Hartree/Bohr. Stationary points on the potential energy surface were identified by frequency calculations at 1 atm and 298.15 K. All optimizations and frequency calculations were performed using the Solvation Model Density (SMD) of Truhlar and coworkers.[29] The transition states were identified by their single imaginary frequencies, whereas reactants, intermediates and products show no imaginary frequency. Reaction paths were confirmed by IRC analysis at the at the SMD/ωB97X-D/6-

31+G(d,p) using the default parameters implemented in Gaussian 09 starting from transition states. The global minimum for 1a was located on the relaxed potential energy surface constructed by varying the dihedral angles between both aromatic rings and the amide plane (Figure S4). Reported relative Gibbs free energies were calculated by taking the difference between the sum of electronic and thermal free energies ($\varepsilon_0 + G_{corr}$) of stationary points.

Molecular dynamics simulations were performed using the pmemd.cuda software from AMBER 18[30] in a NVidia GTX 1070 graphic card. The GAFF force field[31] and TIP3P water model[32] were used. From global minimum structure 1a, the atomic partial charges were calculated with RESP[33] procedure, Antechamber[34] and Gaussian 09 softwares.[28] This structure was solvated in a periodic orthorhombic box with 1651 waters and approximately 40x35x35 Å$^3$ (after equilibration) and more than 20 Å from a periodic image. Chloride counter ions were added to neutralize the total charge of the box using the TIP3P-specific ion parameters from Joung and Cheatham.[35] The production phase was simulated in an NPT ensemble, Langevin thermostat[36] 298.15 K, $\gamma = 1$ ps$^{-1}$, Monte Carlo barostat,[37] Lennard-Jones cutoff 9 Å and Particle Mesh Ewald (PME) long-range eletrostatic algorithm.[38] Because we were interested in conformational states involving hydrogen atoms, no acceleration algorithms involving hydrogen were used, so the time step was 0.5 fs. All the trajectory analyses were performed using the CPPTRAJ V4.20.2 software.[39]

**General Procedure for the Synthesis of Substrate.** Preparation of 2-phthaloimidobenzoic acid (2PIB) and 2-carboxyphthalanilic acid (2CPA). The procedure was adapted from Wiklund et al.[40]

*2-phthaloimidobenzoic acid* (2PIB). In a round bottom flask 6 mL of acetic acid were heated to reflux (oil bath, 120 °C). Then phthalic anhydride (1.48 g, 10 mmol) and anthranilic acid (1.25 g, 9.09 mmol) were added. The reaction was refluxed for 15 hours. After cooling to room temperature, the crude mixture was poured into 10 mL of distilled $H_2O$ and the precipitate formed was filtered, washed with water and dried under reduced pressure yielding the pure imide (2PIB). Yield = 1.28 g (53 %), gray solid. m.p. = 216-218°C. $^1$H NMR (200 MHz, DMSO-$d_6$) δ 13.13 (br s, 1H), 8.07 (d, $J$ = 7.6 Hz, 1H), 8.02-7.90 (m, 4H), 7.78 (t, $J$ = 7.5 Hz, 1H), 7.65 (d, $J$ = 7.6 Hz, 1H), 7.56 (d, $J$ = 7.8 Hz, 1H). $^{13}$C{1H} NMR (50 MHz, DMSO-$d_6$) δ 167.1, 166.1, 134.8, 133.0, 131.8, 131.5, 131.0, 130.7, 129.3, 123.5. FTIR (cm$^{-1}$): 3093 (br, w), 2752 (w), 2610 (w), 1725, 1699, 1601, 1494, 1387, 1293, 1281, 1235, 1117, 1071, 895, 756, 718.

*2-carboxyphthalanilic acid* (2CPA). In a round bottom flask 6 mL of distilled water, 2PIB (300 mg, 1.12 mmol) and 4 equivalents of NaOH (179 mg, 4.49 mmol) were stirred at room temperature for 18 hours. The brownish solution was acidified (pH < 2) with conc. HCl giving a precipitate that was filtered, washed with HCl 0.2 M and dried under reduced pressure. Yield = 270 mg (84 %), white solid. m.p. = 165-167°C. $^{1}$H NMR (200 MHz, DMSO-$d_6$) δ 13.40 (br s, 2H), 11.56 (s, 1H), 8.64 (d, $J$ = 8.3 Hz, 1H), 8.04 (d, $J$ = 7.8 Hz, 1H), 7.89 (d, $J$ = 7.0 Hz, 1H), 7.71-7.59 (m, 4H), 7.22 (t, $J$ = 7.6 Hz, 1H). $^{13}$C{1H} NMR (50 MHz, DMSO-$d_6$) δ 169.7, 167.6, 167.0, 141.1, 138.1, 134.2, 131.9, 131.2, 130.6, 130.2, 129.8, 127.3, 123.0, 119.9, 116.5. FTIR (cm$^{-1}$): 3039 (br), 2646 (w), 2598 (w), 1716, 1687, 1637, 1607, 1590, 1533, 1454, 1366, 1326, 1227, 1154, 757, 726.

## ASSOCIATED CONTENT

### Supporting Information

Spectroscopic data (UV-Vis analysis, $^{1}$H, $^{13}$C{1H} NMR spectra and FTIR), activation parameters, relaxed potential energy surface for 2CPA monoanion, additional IRC plots, Cartesian coordinates for all DFT structures and analysis of molecular dynamics trajectory data.

## AUTHOR INFORMATION

Corresponding Authors
E-mail: bruno.souza@ufsc.br
E-mail: menger@emory.edu

### Notes

The authors declare no competing financial interest.

## ACKNOWLEDGMENTS

This study was financed in part by the Coordenação de Aperfeiçoamento de Pessoal de Nível Superior - Brasil (CAPES) - Finance Code 001. We are also grateful to INCT-Catálise, FAPESC and CNPq for financial support.

## REFERENCES


(1) Menger, F. M. On the Source of Intramolecular and Enzymatic Reactivity. *Acc. Chem. Res.* **1985**, *18* (5), 128–134.

(2) Menger, F. M. Enzyme Reactivity from an Organic Perspective. *Acc. Chem. Res.* **1993**, *26* (4), 206–212.

(3) Menger, F. M.; Galloway, A. L.; Musaev, D. G. Relationship between Rate and Distance. *Chem. Commun.* **2003**, No. 18, 2370–2371.

(4) Souza, B. S.; Mora, J. R.; Wanderlind, E. H.; Clementin, R. M.; Gesser, J. C.; Fiedler, H. D.; Nome, F.; Menger, F. M. Transforming a Stable Amide into a Highly Reactive One: Capturing the Essence of Enzymatic Catalysis. *Angew. Chem.-Int. Ed.* **2017**, *56* (19), 5345–5348.

(5) McClelland, R. A. Benzamide Oxygen Exchange Concurrent with Acid Hydrolysis. *J. Am. Chem. Soc.* **1975**, *97* (18), 5281–5282.

(6) Krzemińska, A.; Moliner, V.; Świderek, K. Dynamic and Electrostatic Effects on the Reaction Catalyzed by HIV-1 Protease. *J. Am. Chem. Soc.* **2016**, *138* (50), 16283–16298.

(7) Bjelic, S.; Åqvist, J. Catalysis and Linear Free Energy Relationships in Aspartic Proteases. *Biochemistry (Mosc.)* **2006**, *45* (25), 7709–7723.

(8) Brik, A.; Wong, C. H. HIV-1 Protease: Mechanism and Drug Discovery. *Org. Biomol. Chem.* **2003**, *1* (1), 5–14.

(9) Menger, F. M.; Nome, F. Interaction vs Preorganization in Enzyme Catalysis. A Dispute That Calls for Resolution. *ACS Chem. Biol.* **2019**, *14* (7), 1386–1392.

(10) Bender, M. L.; Chow, Y.-L.; Chloupek, F. Intramolecular Catalysis of Hydrolytic Reactions. II. The Hydrolysis of Phthalamic Acid1,2. *J. Am. Chem. Soc.* **1958**, *80* (20), 5380–5384.

(11) Kirby, A. J.; Lancaster, P. W. Structure and Efficiency in Intramolecular and Enzymic Catalysis - Catalysis of Amide Hydrolysis by Carboxy-Group of Substituted Maleamic Acids. *J. Chem. Soc.-Perkin Trans. 2* **1972**, No. 9, 1206–1214.

(12) Menger, F. M.; Ladika, M. Fast Hydrolysis of an Aliphatic Amide at Neutral pH and Ambient Temperature. A Peptidase Model. *J. Am. Chem. Soc.* **1988**, *110* (20), 6794–6796.

(13) Morawetz, H.; Shafer, J. Intramolecular Bifunctional Catalysis of Amide Hydrolysis. *J. Am. Chem. Soc.* **1962**, *84* (19), 3783–3784.

(14) Barros, T. C.; Yunes, S.; Menegon, G.; Nome, F.; Chaimovich, H.; Politi, M. J.; Dias, L. G.; Cuccovia, I. M. Hydrolysis of 1,8-and 2,3-Naphthalic Anhydrides and the Mechanism of Cyclization of 1,8-Naphthalic Acid in Aqueous Solutions. *J. Chem. Soc.-Perkin Trans. 2* **2001**, No. 12, 2342–2350.

(15) Andrés, G. O.; Granados, A. M.; de Rossi, R. H. Kinetic Study of the Hydrolysis of Phthalic Anhydride and Aryl Hydrogen Phthalates. *J. Org. Chem.* **2001**, *66* (23), 7653–7657.

(16) Fersht, A. R.; Kirby, A. J. Intramolecular General Acid Catalysis of Ester Hydrolysis by the Carboxylic Acid Group. *J. Am. Chem. Soc.* **1967**, *89* (23), 5961–5962.

(17) Fife, T. H.; Singh, R.; Bembi, R. Intramolecular General Base Catalyzed Ester Hydrolysis. The Hydrolysis of 2-Aminobenzoate Esters. *J. Org. Chem.* **2002**, *67* (10), 3179–3183.

(18) Souza, B. S.; Nome, F. Importance of Equilibrium Fluctuations between Most Stable Conformers in the Control of the Reaction Mechanism. *J. Org. Chem.* **2010**, *75* (21), 7186–7193.

(19) da Silva, P. L.; Guimarães, L.; Pliego, J. R. Revisiting the Mechanism of Neutral Hydrolysis of Esters: Water Autoionization Mechanisms with Acid or Base Initiation Pathways. *J. Phys. Chem. B* **2013**, *117* (21), 6487–6497.

(20) Lightstone, F. C.; Bruice, T. C. Ground State Conformations and Entropic and Enthalpic Factors in the Efficiency of Intramolecular and Enzymatic Reactions. 1. Cyclic Anhydride Formation by Substituted Glutarates, Succinate, and 3,6-Endoxo-$\Delta^4$-Tetrahydrophthalate Monophenyl Esters. *J. Am. Chem. Soc.* **1996**, *118* (11), 2595–2605.

(21) Chai, J.-D.; Head-Gordon, M. Systematic Optimization of Long-Range Corrected Hybrid Density Functionals. *J. Chem. Phys.* **2008**, *128*, 084106.

(22) Chai, J.-D.; Head-Gordon, M. Long-Range Corrected Hybrid Density Functionals with Damped Atom–atom Dispersion Corrections. *Phys. Chem. Chem. Phys.* **2008**, *10* (44), 6615–6620.

(23) McLean, A. D.; Chandler, G. S. Contracted Gaussian-Basis Sets for Molecular Calculations .1. 2nd Row Atoms, Z=11-18. *J. Chem. Phys.* **1980**, *72* (10), 5639–5648.

(24) Clark, T.; Chandrasekhar, J.; Spitznagel, G. W.; Schleyer, P. V. Efficient Diffuse Function-Augmented Basis Sets for Anion Calculations. III. The 3-21+G Basis Set for First-Row Elements, Li-F. *J. Comput. Chem.* **1983**, *4* (3), 294–301.

(25) Frisch, M. J.; Pople, J. A.; Binkley, J. S. Self-Consistent Molecular-Orbital Methods .25. Supplementary Functions For Gaussian-Basis Sets. *J. Chem. Phys.* **1984**, *80* (7), 3265–3269.

(26) Krishnan, R.; Binkley, J. S.; Seeger, R.; Pople, J. A. Self-Consistent Molecular-Orbital Methods .20. Basis Set for Correlated Wave-Functions. *J. Chem. Phys.* **1980**, *72* (1), 650–654.

(27) Krishnan, R.; Frisch, M. J.; Pople, J. A. Contribution of Triple Substitutions to the Electron Correlation-Energy In 4th Order Perturbation-Theory. *J. Chem. Phys.* **1980**, *72* (7), 4244–4245.

(28) M. J. Frisch, G. W. Trucks, H. B. Schlegel, G. E. Scuseria, M. A. Robb, J. R. Cheeseman, G. Scalmani, V. Barone, B. Mennucci, G. A. Petersson, H. Nakatsuji, M. Caricato, X. Li, H. P. Hratchian, A. F. Izmaylov, J. Bloino, G. Zheng, J. L. Sonnenberg, M. Hada, M. Ehara, K. Toyota, R. Fukuda, J. Hasegawa, M. Ishida, T. Nakajima, Y. Honda, O. Kitao, H. Nakai, T. Vreven, J. A. Montgomery, Jr., J. E. Peralta, F. Ogliaro, M. Bearpark, J. J. Heyd, E. Brothers, K. N. Kudin, V. N. Staroverov, R. Kobayashi, J. Normand, K. Raghavachari, A. Rendell, J. C. Burant, S. S. Iyengar, J. Tomasi, M. Cossi, N. Rega, J. M. Millam, M. Klene, J. E. Knox, J. B. Cross, V. Bakken, C. Adamo, J. Jaramillo, R. Gomperts, R. E. Stratmann, O. Yazyev, A. J. Austin, R. Cammi, C. Pomelli, J. W. Ochterski, R. L. Martin, K. Morokuma, V. G. Zakrzewski, G. A. Voth, P. Salvador, J. J. Dannenberg, S. Dapprich, A. D. Daniels, O. Farkas, J. B. Foresman, J. V. Ortiz, J. Cioslowski, and D. J. Fox, Gaussian, Inc., Wallingford CT, 2009.

(29) Marenich, A. V.; Cramer, C. J.; Truhlar, D. G. Universal Solvation Model Based on Solute Electron Density and on a Continuum Model of the Solvent Defined by the Bulk Dielectric Constant and Atomic Surface Tensions. *J. Phys. Chem. B* **2009**, *113* (18), 6378–6396.

(30) D.A. Case, I.Y. Ben-Shalom, S.R. Brozell, D.S. Cerutti, T.E. Cheatham, III, V.W.D. Cruzeiro, T.A. Darden, R.E. Duke, D. Ghoreishi, M.K. Gilson, H. Gohlke, A.W. Goetz, D. Greene, R Harris, N. Homeyer, S. Izadi, A. Kovalenko, T. Kurtzman, T.S. Lee, S. LeGrand, P. Li, C. Lin, J. Liu, T. Luchko, R. Luo, D.J. Mermelstein, K.M. Merz, Y. Miao, G. Monard, C. Nguyen, H. Nguyen, I. Omelyan, A. Onufriev, F. Pan, R. Qi, D.R. Roe, A. Roitberg, C. Sagui, S. Schott-Verdugo, J. Shen, C.L. Simmerling, J. Smith, R. Salomon-Ferrer, J. Swails, R.C. Walker, J. Wang, H. Wei, R.M. Wolf, X. Wu, L. Xiao, D.M. York and P.A. Kollman. *AMBER 2018*; University of California: San Francisco.

(31) M. J. Frisch, G. W. Trucks, H. B. Schlegel, G. E. Scuseria, M. A. Robb, J. R. Cheeseman, G. Scalmani, V. Barone, B. Mennucci,; G. A. Petersson, H. Nakatsuji, M. Caricato, X. Li, H. P. Hratchian, A. F. Izmaylov, J. Bloino, G. Zheng, J. L. Sonnenberg, M. Hada,; M. Ehara, K. Toyota, R. Fukuda, J. Hasegawa, M. Ishida, T.

Nakajima, Y. Honda, O. Kitao, H. Nakai, T. Vreven, J. A. Montgomery, Jr.,; J. E. Peralta, F. Ogliaro, M. Bearpark, J. J. Heyd, E. Brothers, K. N. Kudin, V. N. Staroverov, R. Kobayashi, J. Normand, K. Raghavachari, A. Rendell, J. C. Burant, S. S. Iyengar, J. Tomasi,; M. Cossi, N. Rega, J. M. Millam, M. Klene, J. E. Knox, J. B. Cross, V. Bakken, C. Adamo, J. Jaramillo, R. Gomperts, R. E. Stratmann,; O. Yazyev, A. J. Austin, R. Cammi, C. Pomelli, J. W. Ochterski, R. L. Martin, K. Morokuma, V. G. Zakrzewski, G. A. Voth,; P. Salvador, J. J. Dannenberg, S. Dapprich, A. D. Daniels, O. Farkas, J. B. Foresman, J. V. Ortiz, J. Cioslowski, and D. J. Fox,; Wang, J. Development and Testing of a General Amber Force Field. *J. Comput. Chem.* **2004**, *25* (9), 1157–1174.

(32) Jorgensen, W. L.; Chandrasekhar, J.; Madura, J. D.; Impey, R. W.; Klein, M. L. Comparison of Simple Potential Functions for Simulating Liquid Water. *J. Chem. Phys.* **1983**, *79* (2), 926–935.

(33) Bayly, C. I.; Cieplak, P.; Cornell, W.; Kollman, P. A. A Well-Behaved Electrostatic Potential Based Method Using Charge Restraints for Deriving Atomic Charges: The RESP Model. *J. Phys. Chem.* **1993**, *97* (40), 10269–10280.

(34) Wang, J.; Wang, W.; Kollman, P. A.; Case, D. A. Antechamber: An Accessory Software Package for Molecular Mechanical Calculations. *J Am Chem Soc* **2001**, *222*, U403.

(35) Joung, I. S.; Cheatham, T. E. Determination of Alkali and Halide Monovalent Ion Parameters for Use in Explicitly Solvated Biomolecular Simulations. *J. Phys. Chem. B* **2008**, *112* (30), 9020–9041.

(36) Loncharich, R. J.; Brooks, B. R.; Pastor, R. W. Langevin Dynamics of Peptides: The Frictional Dependence of Isomerization Rates of N-Acetylalanyl-N'-methylamide. *Biopolymers* **1992**, *32* (5), 523–535.

(37) Åqvist, J.; Wennerström, P.; Nervall, M.; Bjelic, S.; Brandsdal, B. O. Molecular Dynamics Simulations of Water and Biomolecules with a Monte Carlo Constant Pressure Algorithm. *Chem. Phys. Lett.* **2004**, *384* (4), 288–294.

(38) Darden, T.; York, D.; Pedersen, L. Particle Mesh Ewald: An N·log(N) Method for Ewald Sums in Large Systems. *J. Chem. Phys.* **1993**, *98* (12), 10089–10092.

(39) Roe, D. R.; Cheatham, T. E. PTRAJ and CPPTRAJ: Software for Processing and Analysis of Molecular Dynamics Trajectory Data. *J. Chem. Theory Comput.* **2013**, *9* (7), 3084–3095.

(40) Wiklund, P.; Romero, I.; Bergman, J. Products from Dehydration of Dicarboxylic Acids Derived from Anthranilic Acid. *Org. Biomol. Chem.* **2003**, *1* (19), 3396–3403.

**For Table of Contents Only**